Preliminary version – final version appeared in
R. Mester, M. Felsberg, editors, Pattern Recognition, Lecture Notes in Computer Science, vol. 6835, 316–325, Springer, Berlin, 2011.

Simultaneous Interpolation and Deconvolution Model for the 3-D Reconstruction of Cell Images

Ahmed Elhayek[1], Martin Welk[2], and Joachim Weickert[3]

[1] Max Planck Institute for Computer Science
Stuhlsatzenhausweg 85, 66123 Saarbrücken, Germany
elhayek@mpi-inf.mpg.de
[2] University for Health Sciences, Medical Informatics and Technology
Eduard-Wallnöfer-Zentrum 1, 6060 Hall/Tyrol, Austria
martin.welk@umit.at, http://ibia.umit.at
[3] Mathematical Image Analysis Group
Campus E1.1, Saarland University, 66041 Saarbrücken, Germany
weickert@mia.uni-saarland.de, http://www.mia.uni-saarland.de

Abstract. Fluorescence microscopy methods are an important imaging technique in cell biology. Due to their depth sensitivity they allow a direct 3-D imaging. However, the resulting volume data sets are undersampled in depth, and the 2-D slices are blurred and noisy. Reconstructing the full 3-D information from these data is therefore a challenging task, and of high relevance for biological applications. We address this problem by combining deconvolution of the 3-D data set with interpolation of additional slices in an integrated variational approach. Our novel 3-D reconstruction model, Interpolating Robust and Regularised Richardson-Lucy reconstruction (IRRRL), merges the Robust and Regularised Richardson-Lucy deconvolution (RRRL) from [16] with variational interpolation. In this paper we develop the theoretical approach and its efficient numerical implementation using Fast Fourier Transform and a coarse-to-fine multiscale strategy. Experiments on confocal fluorescence microscopy data demonstrate the high restoration quality and computational efficiency of our approach.

1 Introduction

Imaging science and cell biology have been interwoven since the beginnings of both fields, when Robert Hooke discovered plant cells with the help of a microscope [9, Observ. XVIII]. In their continual symbiosis, virtually every advance in each of the two fields has been inherently linked with the progress of the other discipline. More than three centuries after Hooke, cell biology forms one of the keystones of today's life sciences, and it continues to pose exciting challenges for imaging science.

Three-dimensional imaging of intracellular structures in living cells is one of these problems. Its solution is of utmost importance for the understanding of life processes, or influences that interfere with these life processes. For example, nanoparticles play an increasing role in modern technology, but their inflammatory and toxicological effects in human cells are hardly understood. This drives the interest of researchers to study the effects of nanoparticles within cells. Tracing the transport of those tiny objects in a living cell is an important part of this research.

While some well-established tools of 3-D imaging such as tomographic methods turn out impractical for imaging living specimens on the desired scale, one of the most promising approaches in current imaging that is compatible with the requirements of this application field are fluorescence microscopy techniques such as Confocal Laser Scanning Microscopy (CLSM) [12] or Stimulated Emission Depletion Microscopy (STED) [8]. Due to physical limitations, however, these methods have much lower resolution in depth direction than within a constant depth plane. Also, light contributions from out-of-focus planes cannot be completely suppressed. The low light intensities involved lead to Poisson noise.

One obtains therefore blurred and noisy data that are severely undersampled in depth direction. To make them suitable for further analysis in biological research, they need to be sharpened, denoised, and interpolated to approximately isotropic resolution. Since measured volumes range up to about $1600 \times 1600 \times 50$ voxels, computationally efficient algorithms are needed.

Related work. Deconvolution has been in the focus of image processing research for a long time. An early and still popular approach is the Richardson-Lucy algorithm [13, 10]. Variational deconvolution methods have been introduced in the nineties [11]. The minimisation interpretation of Richardson-Lucy deconvolution [14] establishes a relation between both approaches that has been used to establish Richardson-Lucy type methods with regularisation [2], specifically in variational formulation [5, 16]. Deconvolution of confocal microscopy images has been considered recently e.g. in [5, 6].

Variational formulations for interpolation have been considered in [3, 15]. A joint variational approach for (blind) deconvolution and interpolation of missing image information (inpainting) has been proposed in [4]. A variational framework for simultaneous deblurring and motion estimation has been proposed in [1].

Our contribution. To address the multiple degradation of fluorescence microscopy imagery of living cells, we propose a novel variational method for simultaneous deconvolution and interpolation in 3-D. By choosing as deconvolution component the modified Richardson-Lucy approach of the type of [5, 16], we obtain an efficient fixed point iteration for minimisation.

Structure of the paper. In Section 2 we develop our joint variational deconvolution and interpolation approach, and derive the fixed point iteration for its optimisation. Its space-discrete numerical realisation is addressed in Section 3. Section 4 presents experimental results on confocal microscopy data to demonstrate the reconstruction quality and efficiency of the model. We end with conclusions in Section 5.

2 Joint Variational Interpolation and Deconvolution

In this section, we present our model for simultaneous interpolation and deconvolution. It combines variational interpolation methods [3, 15] with the deconvolution model from [16]. The advantage of the latter is that it leads to a computationally efficient fixed point iteration similar to Richardson-Lucy deconvolution, called Robust and Regularised Richardson-Lucy deconvolution. Computational efficiency is crucial since we aim at reconstructing large fluorescence microscopy 3-D data sets.

2.1 Deconvolution Model

The deconvolution model from [16] is a modification of the popular Richardson-Lucy (RL) algorithm [10, 13] which is also in broad use for fluorescence microscopy 3-D deconvolution, due to its simplicity and computational efficiency. Let the degraded image f, the sharp image u, and the point-spread-function (PSF) h be smooth functions over $\Omega = \mathbb{R}^3$ (or $\mathbb{R}^2$ for 2D images). Then RL generates a sequence of successively sharpened images $u^1, u^2, ...$ from the initial image $u^0 := f$ via the fixed point iteration

$$u^{k+1} = \left(h^* * \frac{f}{u^k * h} \right) \cdot u^k \ . \tag{1}$$

Here, we denote by h^* the adjoint of the PSF, $h^*(\boldsymbol{x}) := h(-\boldsymbol{x})$. In the case of a noise-free observed image (where $f = g * h$ is satisfied exactly), the multiplier $h^* * \frac{f}{g*h}$ equals 1. Thus, the sharp image g is a fixed point of (1) in this case.

The single parameter of this method is the number of iterations. With more iterations, the degree of sharpening increases, but at the same time the amount of regularisation sinks. In the presence of (even very low) noise the results will be dominated by amplified noise after some number of iterations.

The fixed point iteration (1) is associated with the minimisation of the functional

$$E_{f,h}[u] := \int_\Omega \left(u * h - f - f \ln \frac{u * h}{f} \right) \mathrm{d}\boldsymbol{x} \tag{2}$$

with respect to a *multiplicative* perturbation, thus slightly adapting the usual Euler-Lagrange formalism. This variational viewpoint allows to modify RL by introducing additional regularisers [5, 16] that provide a more flexible means of structure-preserving or structure-enhancing regularisation than the original regularisation by stopping. Moreover, robust data terms can be introduced [16]. With both modifications and the abbreviation $r_f(v) := v - f - f \ln(v/f)$, the energy functional reads

$$E_{f,h}[u] = \int_\Omega \Phi \left(r_f(u * h) \right) + \alpha \, \Psi \left(|\nabla u|^2 \right) \mathrm{d}\boldsymbol{x} \tag{3}$$

where both $\Phi, \Psi : \mathbb{R}^+ \to \mathbb{R}$ are increasing penalty functions, and the regularisation weight α should be chosen dependent on the noise level in the blurred image. The robust data term not only handles extreme noise, but also copes with imprecisions in the blur model and the PSF. Assuming multiplicative perturbation, one can derive from (3) an Euler-Lagrange equation and finally the fixed point iteration, cf. [16]

$$u^{k+1} = \frac{h^* * \left(\Phi'(r_f(u^k * h)) \left(\frac{f}{u^k * h} \right) \right) + \alpha \left[\mathsf{div} \left(\Psi'(|\nabla u^k|^2) \nabla u^k \right) \right]_+}{h^* * \Phi'(r_f(u^k * h)) - \alpha \left[\mathsf{div} \left(\Psi'(|\nabla u^k|^2) \nabla u^k \right) \right]_-} u^k \tag{4}$$

where $[z]_\pm := \frac{1}{2}(z \pm |z|)$. This iteration is called *robust and regularised Richardson-Lucy deconvolution (RRRL)*. It achieves an image restoration quality comparable to state-of-the-art variational deconvolution at a computational cost comparable to that of the original RL method, see [16].

2.2 Interpolation Model

In the interpolation part of our approach, we tie up to PDE models for interpolation and variational image regularisation as were formulated in [3, 15].

Assume that image data is observed in the region $D \subset \Omega$ and is to be extended to the entire domain Ω. Taking into account that image data on D are also contaminated by noise, minimisation of the functional

$$E[u] = \frac{1}{2} \int_D |u - f|^2 \, \mathrm{d}\boldsymbol{x} + \alpha \int_\Omega \Psi(|\nabla u|^2) \, \mathrm{d}\boldsymbol{x} \tag{5}$$

performs simultaneous interpolation and denoising, see [3] with total variation regulariser $\Psi(s^2) = |s|$. The use of a non-quadratic penaliser Ψ ensures that edges are preserved. For $D = \Omega$, variational denoising is recovered.

2.3 Joint Model

To achieve simultaneous interpolation and deconvolution, we proceed in a similar manner as in [4] where a blind deconvolution approach with quadratic penalisation in the data term was combined with TV inpainting. We replace the simple data term of (5) with the deconvolution data term from (3) but evaluate it on the observed domain D only as in (5). The regulariser is inherited from (5) and acts therefore throughout Ω. We aim therefore at minimising the functional

$$E[u] = \int_D \underbrace{\Phi\left(r_f(u * h)\right)}_{\text{data}} \, \mathrm{d}\boldsymbol{x} + \alpha \int_\Omega \underbrace{\Psi(|\nabla u|^2)}_{\text{smoothness}} \, \mathrm{d}\boldsymbol{x} \, . \tag{6}$$

Similar as before, the data term herein suppresses deviations from the blur model in the observed image domain D by asymmetric penalisation of the reconstruction error. The smoothness term combines structure-preserving denoising in D with structure-preserving interpolation in $\Omega \setminus D$. One should, however, be aware that due to the convolutions also the direct influence of the data term is not limited to D. The regularisation weight $\alpha > 0$ balances the influence of the data and smoothness terms.

In order to compute the minimiser u, we derive again the Euler-Lagrange equation for a multiplicative perturbation. As in the case of RRRL, this proceeding not only allows to derive an efficient RL-style fixed point iteration but also ensures that the positivity of u is strictly preserved. Denoting by χ_D the characteristic function of D, the resulting equation reads

$$\left(h^* * \left(\chi_D \Phi'(r_f(u * h)) \left(1 - \frac{f}{u * h} \right) \right) - \alpha \, \mathsf{div} \left(\Psi'(|\nabla u|^2) \nabla u \right) \right) \cdot u = 0 \, , \tag{7}$$

from which we obtain the fixed point iteration

$$u^{k+1} = \frac{h^* * \left(\chi_D \Phi'(r_f(u^k * h)) \left(\frac{f}{u^k * h} \right) \right) + \alpha \left[\mathsf{div} \left(\Psi'(|\nabla u^k|^2) \nabla u^k \right) \right]_+}{h^* * \left(\chi_D \Phi'(r_f(u^k * h)) \right) - \alpha \left[\mathsf{div} \left(\Psi'(|\nabla u^k|^2) \nabla u^k \right) \right]_-} u^k \, . \tag{8}$$

We will call this iteration *simultaneous interpolation and RRRL deconvolution (IRRRL)*. It converges to the steady-state much faster than gradient descent schemes, which are often used for conventional variational approaches, see [4] for simultaneous interpolation and deconvolution. This will make our method computationally more efficient than conventional approaches, while at the same time it achieves reconstruction quality comparable to those approaches.

We remark that classic RL deconvolution [10, 13] as well as regularised RL [5], robust RL [16] and RRRL [16] are embedded as special cases in IRRRL. An extension to multi-channel image data is straightforward along the lines of [16]. For more details we refer to [7].

3 Numerical Aspects

To implement IRRRL for the reconstruction of 3-D images, a discretised version of (8) is required. In the discretisation of the data terms (i.e. the first term in the numerator and the first term denominator) at voxel (i, j, l) the expensive 3-D convolution operations are transferred to the Fourier domain. In order to use a Fast Fourier Transform (FFT) implementation for which image dimensions need to be powers of two, and to mitigate wraparound errors, images are extended by mirroring within a suitable stripe around the image domain. The Fourier strategy considerably improves the computational efficiency of our model over the direct implementation of the convolutions in the spatial domain. The characteristic function χ_D is implemented using a binary image.

For the diffusion term $D := \mathsf{div}\,(g\,\nabla u)$, we found that the discretisation method does not have a major effect on the performance of our model. Thus, we use the simplest discretisation based on central differences:

$$\begin{aligned} &D_{i,j,l} \\ &= \frac{1}{h_1}\left(\frac{g_{i+1,j,l}+g_{i,j,l}}{2}\,\frac{u_{i+1,j,l}-u_{i,j,l}}{h_1} - \frac{g_{i,j,l}+g_{i-1,j,l}}{2}\,\frac{u_{i,j,l}-u_{i-1,j,l}}{h_1}\right) \\ &+ \frac{1}{h_2}\left(\frac{g_{i,j+1,l}+g_{i,j,l}}{2}\,\frac{u_{i,j+1,l}-u_{i,j,l}}{h_2} - \frac{g_{i,j,l}+g_{i,j-1,l}}{2}\,\frac{u_{i,j,l}-u_{i,j-1,l}}{h_2}\right) \\ &+ \frac{1}{h_3}\left(\frac{g_{i,j,l+1}+g_{i,j,l}}{2}\,\frac{u_{i,j,l+1}-u_{i,j,l}}{h_3} - \frac{g_{i,j,l}+g_{i,j,l-1}}{2}\,\frac{u_{i,j,l}-u_{i,j,l-1}}{h_3}\right), \end{aligned} \tag{9}$$

where h_1, h_2, and h_3 are the spatial grid sizes in x, y, and z directions, respectively. The diffusivity $g = \Psi'(|\nabla u|^2)$ is discretised by

$$\begin{aligned} g_{i,j,l} = \Psi'\Bigg(&\left(\frac{u_{i+1,j,l}-u_{i-1,j,l}}{2h_1}\right)^2 + \left(\frac{u_{i,j+1,l}-u_{i,j-1,l}}{2h_2}\right)^2 \\ &+ \left(\frac{u_{i,j,l+1}-u_{i,j,l-1}}{2h_3}\right)^2\Bigg). \end{aligned} \tag{10}$$

In order to speed up the computation, we complement the scheme developped so far by a coarse-to-fine strategy. On each level (except the coarsest one), the result of

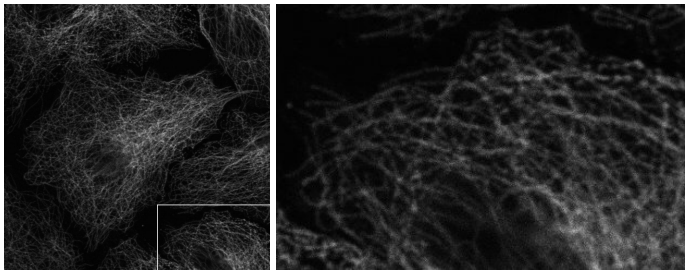

Fig. 1. Confocal microscopy 3-D image of the filament network of a cell. **(a) Left:** Slice 12 from the complete 3-D image ($1024 \times 1024 \times 24$ voxels). **(b) Right:** Corresponding slice from the clipped 3-D image (Dataset A, $376 \times 244 \times 24$ voxels).

the next coarser level serves as a fairly good initialisation, which makes the iteration converge considerably faster.

Since in our case interpolation is used to increase resolution in depth (z) direction, we implemented the coarse-to-fine approach as follows:

1. Downsample the 3-D image to a coarse scale in x, and y directions.
2. Apply the IRRRL fixed point iteration at the coarse version of the image.
3. Interpolate the solution of the coarse level and use it as an initialisation at the next finer scale.

In experiments on 3-D cell images the coarse-to-fine strategy boosts the computational efficiency of IRRRL by more than a factor 4.

4 Experimental Evaluation

In this section, we show experimental results based on real-world data to illustrate the benefits of the proposed simultaneous model. Note that all computations were performed in 3-D although only exemplary slices are displayed. In all models, we use as penalisation functions $\Phi(r) = 2\sqrt{r}$ in the data term, and the Charbonnier function $\Psi(s^2) = 2\lambda\sqrt{1 + s^2/\lambda^2} - 2\lambda$ in the smoothness term.

The data sets used in the experiment are confocal fluorescence microscopy 3-D images of the filament network of living cells. Images and 3-D PSFs were provided by the Nano-Cell Interactions group at the Leibniz Institute for New Materials (INM), Saarbrücken. The resolution of these data sets in z direction is significantly lower than in x and y directions. We aim therefore at deblurring these images and at the same time interpolating a number of additional slices (typically, 1–5 slices) between each pair of neighbouring slices in z direction, in order to compensate the unequal resolution and achieve approximately equal voxel dimensions in x, y, and z directions.

Due to the huge image dimensions, 3-D reconstruction of an entire data set was beyond the memory capacity of available PCs. The experiments presented here were therefore carried out on cutouts. Fig. 1(a), for example, shows Slice 12 of a confocal microscopy data set. Its central part represents the filament network of a complete cell,

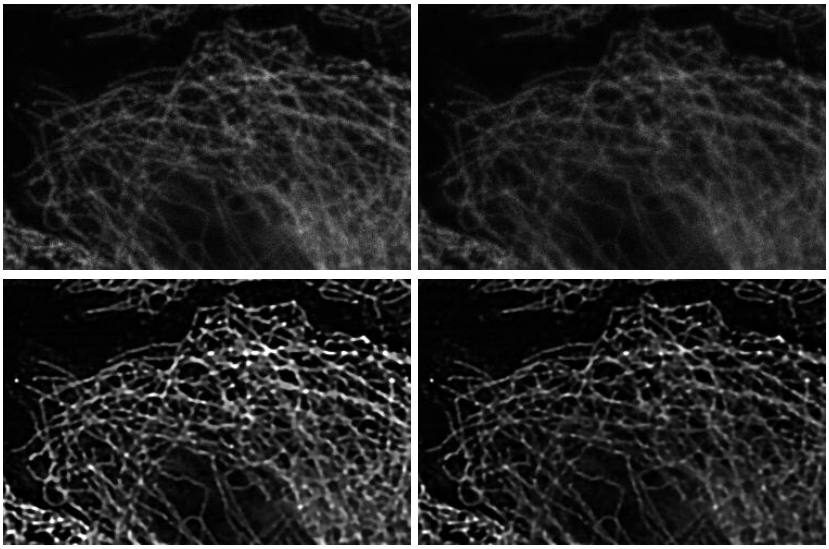

Fig. 2. 3-D reconstruction of Dataset A/2 by 100 iterations of IRRRL with Charbonnier regulariser, $\alpha = 0.002$. **(a) Top left:** Slice 8 of Dataset A/2. **(b) Top right:** Slice 9 of Dataset A/2. **(c) Bottom left:** Reconstruction of Slice 8. **(d) Bottom right:** One of the three slices interpolated between Slices 8 and 9.

while the outer parts belong to adjacent cells. For our experiments, the number of slices was retained but all slices were clipped as shown in Fig. 1(b). In the following, this clipped image will be called Dataset A.

In Dataset A, the voxel size is about $126\,\mathrm{nm}$ in depth and $62\,\mathrm{nm}$ within the constant depth planes. Interpolating a single slice between each pair of subsequent slices would actually suffice to make the voxel dimensions almost equal in x, y, and z directions. For a more informative test of the performance of our method, we remove the even-numbered slices from the data set. We will refer to this thinned dataset as Dataset A/2. To compensate for the thinning, each gap between slices of Dataset A/2 should be filled with three reconstructed slices. On one hand, this makes the problem considerably harder. On the other hand, it enables us to assess the reconstruction quality: Using sharpened versions of the retained slices from Dataset A as ground truth, we can quantify the reconstruction error of the second of three reconstructed slices. To this end, we use the average absolute error (AAE).

Fig. 2 illustrates the result of the first experiment. In (a) and (b) subsequent slices from Dataset A/2 are shown. The reconstruction of the slice in (a) is shown in (c). This demonstrates the deconvolution quality of IRRRL, since details in the processed slice (c) are much sharper than in the original slice (a). This makes it easier to track the filament network of the cell which is essential for microbiological applications like tracing nanoparticle transport in living cells. The interpolation effect of IRRRL is demonstrated in Subfigure (d) by one of the three slices interpolated between (a) and (b).

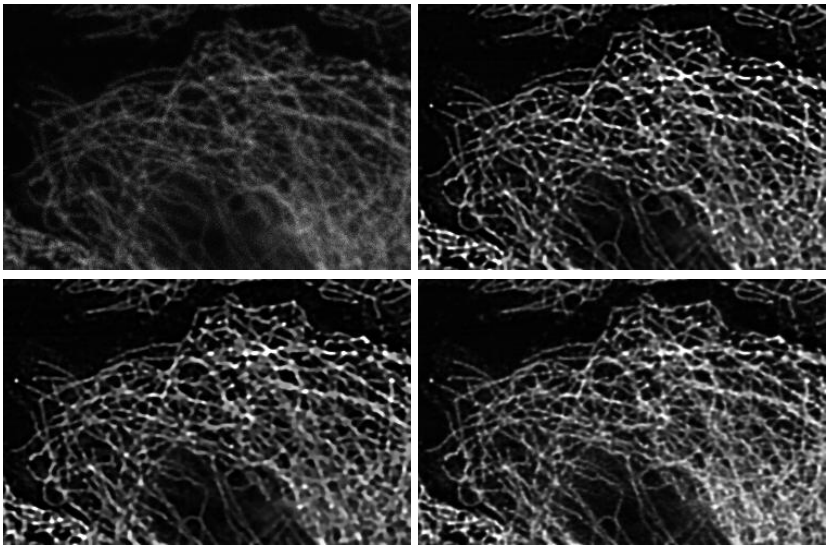

Fig. 3. Comparison with the sequential approach. **(a) Top left:** Slice 14 of Dataset A (not present in Dataset A/2). **(b) Top right:** Ground truth (Slice 14 after the preprocessing step). **(c) Bottom left:** Corresponding interpolated slice from IRRRL reconstruction of Dataset A/2. **(d) Bottom right:** Corresponding interpolated slice from sequential deconvolution and interpolation of Dataset A/2. Note particularly the unsatisfactory reconstruction in the lower right part.

In Fig. 3 we present further results together with a ground-truth comparison. Subfigure (a) shows one of the even-numbered slices of Dataset A which are removed in A/2. The sharpened version shown in Subfigure (b) is taken from an IRRRL reconstruction of the undecimated Dataset A. This slice forms the ground truth for our subsequent comparison. Figure 3(c) shows the second interpolated slice between slices 7 and 8 from our IRRRL reconstruction of the decimated Dataset A/2, which corresponds to Slice 14 of Dataset A. Indeed, the slices in (c) and (b) are not only visually similar, but also the AAE between them amounts to a low 4.55, confirming the good quality of the interpolation. For comparison, the AAE between the sharpened slices 7 and 8 is 16.83.

In our second experiment, we want to demonstrate the advantage of simultaneous interpolation and deconvolution over a *sequential approach* that deconvolves the data first, and then interpolates additional slices. We deconvolve therefore Dataset A/2 by RRRL and then interpolate the three missing slices using the variational interpolation model (5). The result is shown in Fig. 3(d). This image corresponds to the same slice as (b) and (c). The visual impression that the reconstruction quality of (d) is inferior to (c) is confirmed by the AAE of (d) vs. (b) which is 11.4.

A second example of reconstruction by IRRRL is shown in Fig. 4, based on a different dataset.

Finally, in order to illustrate the computational efficiency of IRRRL, we collect in Table 1 runtime measurements of IRRRL and a conventional variational approach for simultaneous deconvolution and interpolation.

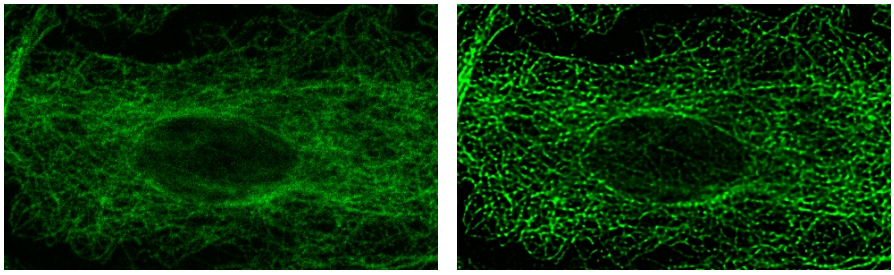

Fig. 4. 3-D reconstruction by IRRRL with Charbonnier regulariser, 100 iterations, $\alpha = 0.001$. **(a) Left**: Slice 5 of a fluorescence microscopy data set (Dataset B, $486 \times 297 \times 22$ voxels). **(b) Right**: Interpolated slice between slices 5 and 6.

We start with the conventional method. It consists essentially in a non-blind variant of the functional from [4] being minimised by gradient descent. For reasonable reconstruction quality, 500 iterations are needed. A straightforward IRRRL implementation speeds up the computation by a factor of more than three. Some increase in the computational cost of a single iteration is more than outbalanced by the reduction of the iteration count to 100 for comparable reconstruction quality.

In both cases so far convolution was computed in the spatial domain. Since the confocal microscopy blur kernel has fairly large spatial dimensions, it is beneficial to use instead an FFT-based convolution via the Fourier domain. In our example, this achieves a speed-up factor of about thirteen. In a last step, we improve this method further by introducing the coarse-to-fine strategy with just two scales, thereby increasing the speed roughly to fourfold.

5 Conclusion and Future Work

We have developped an integrated variational approach for 3-D image deconvolution and interpolation that does not only deliver reconstruction in high quality but also allows efficient numerical implementation by means of a fixed point iteration similar to the Richardson-Lucy algorithm. Further speed-up was achieved by transferring convolution operations to the Fourier domain via FFT, and a coarse-to-fine strategy.

Table 1. Approximate computational expense of the conventional variational simultaneous interpolation and deconvolution model and different implementations of the IRRRL model. Computation times refer to a single-threaded calculation on a Core2Duo CPU running at 2.00 GHz.

Implementation	Iterations	Computation time (m)	Reduction factor w.r.t. conventional implementation
conventional	500	6020	1
Spatial	100	1791	3.36
Fourier-spatial	100	135	44.59
Coarse-to-fine	20-20	33	182.42

Future work will be directed to integrate this method with other image processing tools for 3-D confocal microscopy data into efficient software for cell biological research. Moreover, improvements of the model like edge-enhancing regularisers will be investigated. Concerning the implementation, 3-D image processing is highly demanding in terms of time and memory, so further algorithmic optimisation in both parameters is another topic of ongoing research.

References

1. Bar, L., Berkels, B., Rumpf, M., Sapiro, G.: A variational framework for simultaneous motion estimation and restoration of motion-blurred video. In: Proc. Eleventh International Conference on Computer Vision. Rio de Janeiro, Brazil (Oct 2007)
2. Bratsolis, E., Sigelle, M.: A spatial regularization method preserving local photometry for Richardson-Lucy restoration. Astronomy and Astrophysics 375(3), 1120–1128 (2001)
3. Chan, T.F., Shen, J.: Mathematical models for local nontexture inpaintings. SIAM Mathematics 62, 1019–1043 (2002)
4. Chan, T.F., Yip, A.M., Park, F.E.: Simultaneous total variation image inpainting and blind deconvolution. International Journal of Imaging Systems and Technology 15, 92–102 (2005)
5. Dey, N., Blanc-Feraud, L., Zimmer, C., Roux, P., Kam, Z., Olivo-Marin, J., Zerubia, J.: Richardson-Lucy algorithm with total variation regularization for 3D confocal microscope deconvolution. Microscopy Research and Technique 69(4), 260–266 (2006)
6. Dupé, F.X., Fadili, J., Starck, J.L.: Deconvolution of confocal microscopy images using proximal iteration and sparse representations. In: 5th IEEE International Symposium on Biomedical Imaging: From Nano to Macro. pp. 736–739. Paris (2008)
7. Elhayek, A.: Simultaneous Interpolation and Deconvolution Approach to 3D Reconstruction of Cell Images. Master's thesis, Department of Mathematics and Computer Science, Saarland University, Saarbrücken. (2011)
8. Hell, S.W., Wichmann, J.: Breaking the diffraction resolution limit by stimulated emission: stimulated-emission-depletion fluorescence microscopy. Optics Letters 19(11), 780–782 (1994)
9. Hooke, R.: Micrographia: or Some physiological descriptions of minute bodies made by magnifying glasses. J. Martyn and J. Allestry, London (1665)
10. Lucy, L.: An iterative technique for rectification of observed distributions. The Astronomical Journal 79(6), 745–765 (1974)
11. Osher, S., Rudin, L.: Total variation based image restoration with free local constraints. In: Proc. 1994 IEEE International Conference on Image Processing. pp. 31–35. Austin, Texas (1994)
12. Pawley, J.B. (ed.): Handbook of Biological Confocal Microscopy. Springer, Berlin, 3rd edn. (2006)
13. Richardson, W.H.: Bayesian-based iterative method of image restoration. Journal of the Optical Society of America 62, 55– 59 (1972)
14. Snyder, D., Schulz, T.J., O'Sullivan, J.A.: Deblurring subject to nonnegativity constraints. IEEE Transactions on Image Processing 40(5), 1143–1150 (1992)
15. Weickert, J., Welk, M.: Tensor Field Interpolation with PDEs. In: J. Weickert, H. Hagen (Eds.): Visualization and Processing of Tensor Fields. pp. 315–325. Springer, Berlin (2006)
16. Welk, M.: Robust variational approaches to positivity-constrained image deconvolution. Tech. Rep. 261, Department of Mathematics, Saarland University, Saarbrücken, Germany (March 2010)